Published in final edited form as:
J Neurophysiol. 1999 November ; 82(5): 2765–2775.

Electrophysiological Properties and Synaptic Responses of Cells in the Trigeminal Principal Sensory Nucleus of Postnatal Rats

FU-SUN LO, **WILLIAM GUIDO**, and **REHA S. ERZURUMLU**
Department of Cell Biology and Anatomy and Neuroscience Center of Excellence, Louisiana State University Medical Center, New Orleans, Louisiana 70112

Abstract

In the rodent brain stem trigeminal complex, select sets of neurons form modular arrays or "barrelettes," that replicate the patterned distribution of whiskers and sinus hairs on the ipsilateral snout. These cells detect the patterned input from the trigeminal axons that innervate the whiskers and sinus hairs. Other brain stem trigeminal cells, interbarrelette neurons, do not form patterns and respond to multiple whiskers. We examined the membrane properties and synaptic responses of morphologically identified barrelette and interbarrelette neurons in the principal sensory nucleus (PrV) of the trigeminal nerve in early postnatal rats shortly after whisker-related patterns are established. Barrelette cell dendritic trees are confined to a single barrelette, whereas the dendrites of interbarrelette cells span wider territories. These two cell types are distinct from smaller GABAergic interneurons. Barrelette cells can be distinguished by a prominent transient A-type K^+ current (I_A) and higher input resistance. On the other hand, interbarrelette cells display a prominent low-threshold T-type Ca^{2+} current (I_T) and lower input resistance. Both classes of neurons respond differently to electrical stimulation of the trigeminal tract. Barrelette cells show either a monosynaptic excitatory postsynaptic potential (EPSP) followed by a large disynaptic inhibitory postsynaptic potential (IPSP) or just simply a disynaptic IPSP. Increasing stimulus intensity produces little change in EPSP amplitude but leads to a stepwise increase in IPSP amplitude, suggesting that barrelette cells receive more inhibitory input than excitatory input. This pattern of excitation and inhibition indicates that barrelette cells receive both feed-forward and lateral inhibition. Interbarrelette cells show a large monosynaptic EPSP followed by a small disynaptic IPSP. Increasing stimulus intensity leads to a stepwise increase in EPSP amplitude and the appearance of polysynaptic EPSPs, suggesting that interbarrelette cells receive excitatory inputs from multiple sources. Taken together, these results indicate that barrelette and interbarrelette neurons can be identified by their morphological and functional attributes soon after whisker-related pattern formation in the PrV.

INTRODUCTION

The stereotypic arrangement of whisker follicles and sinus hairs on the snout of nocturnal rodents is replicated by the distribution of presynaptic afferent arbors and their postsynaptic target cells ("barrelettes") in the brain stem trigeminal complex (BSTC) (Bates and Killackey 1985; Belford and Killackey 1979; Erzurumlu et al. 1980; Ma 1993; Ma and Woolsey 1984). Trigeminothalamic projection (barrelette) cells of the principal sensory nucleus of the trigeminal nerve (PrV) relay whisker-specific patterns to the dorsal thalamus

Address for reprint requests: F.-S. Lo, Dept. of Cell Biology and Anatomy, Louisiana State University Medical Center, 1901 Perdido St., New Orleans, LA 70112. .

("barreloids"), and consequently to the primary somatosensory cortex ("barrels") (Belford and Killackey 1980; Durham and Woolsey 1984; Erzurumlu et al. 1980; Erzurumlu and Jhaveri 1990; Erzurumlu and Killackey 1980; Ivy and Killackey 1981; Killackey and Fleming 1985; Ma and Woolsey 1984; Senft and Woolsey 1991; Van der Loos 1976; Woolsey and Van der Loos 1970). This patterned neural organization takes place during a sensitive period in development. Disruptions of the sensory periphery before *postnatal day* (*PND*) *3–4* irreversibly alter central neural patterns (see Erzurumlu and Killackey 1982; Jhaveri and Erzurumlu 1992; O'Leary et al. 1994; Woolsey 1990 for reviews).

Whisker-related primary afferents convey the pattern template to select groups of target neurons at all levels of the trigeminal neuraxis (Erzurumlu and Jhaveri 1990). In the rat, barrelette formation begins shortly before birth and it is consolidated by *PND5* (Belford and Killackey 1980; Chiaia et al. 1992). To understand the mechanisms underlying pattern formation in the mammalian CNS, it is important to distinguish between the structural and functional characteristics of pattern forming neurons and other cells. In this study we focused on the barrelette and interbarrelette neurons in early postnatal rat PrV. Using whole cell patch recording, immunohistochemistry, and intracellular biocytin labeling techniques, we charted out the morphological characteristics, membrane properties, and synaptic circuitry within barrelette region of the PrV of *PND4–12* rat pups. We show that barrelette and interbarrelette cells can be distinguished by their morphological and electrophysiological properties shortly after whisker-related pattern formation. Our analyses of synaptic responses also suggest that barrelette cells receive excitatory input from a single whisker follicle, and a strong lateral inhibition originating from neighboring whiskers. Interbarrelette cells receive excitatory inputs from a variety of sources, including multiple whisker follicles, other interbarrelette or barrelette cells. In both types of cells, the excitation is mediated by *N*-methyl-D-aspartate (NMDA) and non-NMDA receptors, whereas the inhibitory component is mediated by $GABA_A$ receptors.

METHODS

Brain slice preparation

Sprague-Dawley rat pups ranging in age from *PND4* to *12* were deeply anesthetized with Fluothane (Halothane) and then killed by decapitation. The brain was removed quickly and immersed in cold (4°C), sucrose-based artificial cerebrospinal fluid (ACSF, in mM: 234 sucrose, 2.5 KCl, 1.25 NaH_2PO_4, 10 $MgSO_4$, 24 $NaHCO_3$, 11 glucose, and 0.5 $CaCl_2$) bubbled with 95% O_2-5% CO_2, pH 7.4. The brain stem was embedded in 2% agar and cut into 500-μm-thick transverse sections with a vibratome (Electron Microscopy Sciences). Slices containing the trigeminal principal sensory nucleus (PrV) were placed in a submerged-type recording chamber (Fine Science Tools) and continuously perfused (2 ml/min) with normal ACSF (in mM: 124 NaCl, 2.5 KCl, 1.25 NaH_2PO_4, 2 $MgSO_4$, 26 $NaHCO_3$, 10 glucose, and 2 $CaCl_2$, pH 7.4) at room temperature. Bath application of bicuculline (10 μM) or D-2-amino-5-phosphonovaleric acid (D-APV; 50 μM) were used to block $GABA_A$ or NMDA receptors. We also applied Cs^+ (1 mM), Ni^{2+} (200–500 μM) or 4-aminopyridine (4-AP; 1 mM) to block H, T, and A-type conductances. A photomicrograph of the slice preparation placed in the recording chamber is shown in Fig. 1. At the ages tested, the trigeminal tract (TrV) and PrV barrelette region can be readily distinguished.

Electrophysiological methods

Recordings began at least 1 h after incubation in normal ACSF. Whole cell patch micropipettes were pulled horizontally in two stages from borosilicate glass (WPI, K150F-4) with a P-87 puller (Sutter Instrument). The patch electrodes were backfilled with a potassium-based solution (in mM: 140 K-gluconate, 10 HEPES, 1.1 EGTA-Na, 0.1 $CaCl_2$, 2

$MgCl_2$, 2 ATP-Na, and 0.2 GTP-Na, with or without 1% biocytin, pH 7.25) with a tip resistance of 7–10 MΩ. Neurons in the ventral part of the PrV (barrelette region) were blindly patched using the techniques described by Blanton et al. (1989) and Ferster and Jagadeesh (1992). In brief, patch-electrode resistance was monitored in Bridge Mode of Axoclamp 2B amplifier by measuring the voltage drop induced by a current pulse (−100 pA, 200 ms). An increase in resistance of 20–50 MΩ was taken as a sign that the electrode tip contacted the surface of a neuron. A steady negative pressure was applied with a 5-ml syringe to form a gigaohm seal. Then a brief suction was used to break into the cell body. The formation of whole cell configuration was indicated by a sudden drop in seal resistance and a DC drop of >55 mV. After "break-in," the serial resistance was compensated with bridge balance, and junction potential (Neher 1992) was not corrected. We only collected data from cells with resting membrane potential negative to −55 mV and input resistance >300 MΩ. Neuronal activity was digitized with an Instrutek VR10B interface unit and stored on a Macintosh Power PC (9500/132) using *Pulse* (HEKA) software program. For biocytin labeling experiments, we filled the patch electrodes with 1% biocytin dissolved in potassium-based solution. Once membrane properties and synaptic responses were characterized, the cells were filled intracellularly with biocytin by passing AC pulses (±1 nA, 60 ms for each cycle) through the biocytin-filled recording electrode.

A pair of fine-tip stimulating electrodes (0.5 MΩ, WPI, IRM33A05KT) were inserted at various points along the trigeminal tract (TrV) lateral to the ventral PrV (barrelette region). Current pulses (0.2–0.5 ms duration, 0.05–1.0 mA) were passed through the electrodes at 0.33 Hz to evoke postsynaptic potentials. To investigate the voltage dependency of the postsynaptic potentials, DC current was passed through the recording patch electrode to change the membrane potential. Different DC pulse protocols were used to induce active conductances of trigeminal neurons. Each cell's membrane potential was held at −60 mV (except where indicated) to compare voltage-dependent conductances and postsynaptic potentials between different cells.

Identification of excitatory postsynaptic potentials (EPSPs) and inhibitory postsynaptic potentials (IPSPs) was based on their voltage dependency and their responses to glutamate and GABA antagonists. The non-NMDA component of an EPSP increased in amplitude (see Fig. 6*A*) with membrane hyperpolarization, enabling us to distinguish between an EPSP and a shock artifact. EPSPs showed predictable changes in amplitude with changes in membrane potential, whereas shock artifacts did not. The NMDA component of an EPSP was identified by its nonlinear voltage dependency, slow decay time, and blockade by D-APV. The $GABA_A$ receptor–mediated IPSP was identified by its reversal with membrane hyperpolarization (~70 mV), and blockade by bicuculline. The onset of the EPSPs or IPSPs was estimated by superimposing the PSPs at different membrane potentials. Despite the changes in amplitude, the onset of PSPs remained fixed. Additionally, the onset of the IPSP could be estimated by comparing responses in the presence or absence of bicuculline (see Fig. 6*B*).

To investigate stimulus-response relationships, we first determined the threshold of activation (~0.05 mA, 0.3 ms) for postsynaptic potentials. We then increased stimulus intensity progressively until the postsynaptic potential reached its maximal amplitude (approximately <1 mA, 0.3 ms). This procedure was repeated three to five times to ensure that the stepwise increase in amplitude was reliable and not due to fluctuations in EPSP amplitude (see also Allen et al. 1977; Bartlett and Smith 1999; Mock et al. 1997).

Histological methods

One hour after biocytin injection, the slice was fixed by 4% paraformaldehyde in 0.1 M phosphate buffer for 48 h. The fixed slice was transferred into phosphate-buffered saline (PBS) at 4°C and then incubated in 10% methanol + 3% H_2O_2 overnight. After several

rinses in PBS, the slice was reacted with avidin-biotin complex (ABC Elite kit, Vector Laboratories) overnight at 4°C (1:100 in PBS with 1.8% NaCl and 0.5% Triton X-100). The next day, the slice was rinsed again in PBS and 0.1 M acetate buffer (pH 6.0) and incubated in glucose oxidase-nickel ammonium sulfate and diaminobenzidine until the labeled cells could be visualized. The slice was rinsed in acetate buffer and PBS, mounted on a slide, dehydrated, and cover-slipped. Labeled cells were drawn with a drawing tube attached to a Nikon Labophot microscope. Counterstaining for cytochrome oxidase histochemistry (Wong-Riley and Welt 1980) revealed the barrelettes in the PrV of *PND4–12* rat brain stem.

For GABA immunohistochemistry, *PND4–7* pups ($n = 6$) were killed with an overdose of pentobarbital sodium and perfused transcardially with PBS and 4% paraformaldehyde in PBS. The brain stems were taken out, cryoprotected in 30% sucrose in PBS, and frozen sectioned at a thickness of 50 μm. Sections were first soaked in 4% goat serum in PBS (1 h), then in anti-GABA antibody (Eugene Tech. International, dilution 1:2,000) in 1% goat serum and PBS, overnight at room temperature. The next day, sections were rinsed in PBS and incubated in biotinylated goat-anti-guinea pig antibody in PBS (Vector Laboratories, dilution 1:200) for 2 h. After several rinses in PBS, sections were processed with an avidin-biotin complex (Vectastain kit, Vector Laboratories), and the reaction product was visualized with diaminobenzidine. Control sections were processed as described above, but without the primary antibody.

RESULTS

Morphological features of barrelette, interbarrelette, and GABAergic interneurons of the PrV are illustrated in Fig. 2. Using the blind whole cell recording technique, we could study only the medium and large size neurons of PrV, and not the smaller GABAergic cells. GABAergic interneurons are present throughout the nucleus and are found within and between barrelettes (Fig. 2*A*). Interbarrelette neurons are large cells with extensive dendritic trees that span several barrelettes and septae (Fig. 2, *B* and *C*). In contrast, barrelette neurons are smaller cells with shorter dendritic fields confined to a single barrelette domain (Fig. 2, *B* and *E*). These anatomic observations are consistent with previous findings of Arends and Jacquin (1993), who used Lucifer yellow fills to identify barrelette and interbarrelette cells.

Electrophysiological identification of barrelette and interbarrelette cells

We performed whole cell patch recordings from 64 neurons in the barrelette region of the PrV. Of these, 41 had a prominent A-type potassium conductance (I_A) as well as an H-type mixed cation conductance (I_H; Fig. 3*A*). We were able to fill 10 such cells with biocytin, and based on their dendritic morphology they all were barrelette neurons. Additionally these cells all had I_A and I_H. Dendritic fields of five of these cells were reconstructed and plotted against barrelette patches visualized with cytochrome oxidase histochemistry (Fig. 2). The cell illustrated in Fig. 2 (*cell 1*) and Fig. 3*A* showed a depolarizing "sag" during membrane hyperpolarization (indicated by H in Fig. 3*A*). Application of Cs^+ (1 mM, $n = 4$) blocked this inward rectification (Fig. 4*B*), indicating that barrelette cells possess a hyperpolarization-activated I_H. Frequently, at the end of the hyperpolarizing current pulses, a hyperpolarizing tail (~150 ms) was observed (Fig. 3*A*, indicated by A). When the barrelette cell was depolarized (−50 mV) after hyperpolarization (−120 mV), there was a hyperpolarizing notch before the first spike (Fig. 3*B*, indicated by arrow A), which led to a substantial delay in action potential firing. Membrane depolarization led to a train of Na^+ spikes (Fig. 3*B*). As can be seen, the frequency of spikes varied systematically with the intensity of depolarizing current pulses. Application of 4-AP (1 mM, $n = 5$) blocked completely the hyperpolarizing notch (Fig. 4*C*) and decreased the latency of the initial spike, suggesting that these cells possess I_A. Barrelette cells could also be distinguished by their passive membrane properties. The resting membrane potential of barrelette cells was −62.1

± 0.6 mV (mean ± SE, $n = 41$, Fig. 4*A*), and their input resistance was 633 ± 34.7 MΩ ($n = 41$, Fig. 4*A*), the latter confirming the morphological observation that barrelette cells have relatively small soma.

The remaining 23 neurons also exhibited strong I_H (Fig. 3*C*). However, membrane depolarization from a hyperpolarized state evoked a triangular depolarization (Fig. 3, *C* and *D*, indicated by T) with a burst of Na^+ spikes riding on it. Application of Ni^{2+} (200–500 μM, $n = 5$) blocked this response (Fig. 4*D*), suggesting that it is mediated by a low-threshold T-type Ca^{2+} conductance (I_T). We injected biocytin into eight such neurons. All of these cells had large dendritic trees distributed over and in between several barrelettes, and possessed a large I_T. Thus we classified neurons with I_T as interbarrelette cells. The resting membrane potential of interbarrelette cells was −60.4 ± 0.7 mV ($n = 23$), which is not significantly different from that of barrelette cells (Fig. 4*A*). The input resistance of interbarrelette cells was significantly lower (2-tailed *t*-test, $P < 0.0002$) than barrelette cells (417 ± 34.7 MΩ; $n = 23$, Fig. 4*A*), confirming the anatomic observation that interbarrelette cells have larger call bodies than barrelette neurons.

During postnatal development (*PND4–12*), the resting membrane potential and active conductances for both classes of neurons remained largely unchanged. However, we did note that input resistance declined significantly (data not shown). Ongoing studies are aimed to detail developmental changes in electrophysiological properties of PrV cells before, during, and after whisker-specific pattern formation (Erzurumlu and Lo 1999).

Synaptic responses of barrelette cells

Figure 5*A* shows the arrangement of stimulating and recording sites in the brain slice (see also Fig. 1). Previous anatomic studies showed that the rat trigeminal tract fibers are topographically organized from early embryonic ages on (Bates and Killackey 1985; Erzurumlu and Jhaveri 1992; Erzurumlu and Killackey 1982, 1983). This topographic organization has been demonstrated by either lesions of specific whisker rows in perinatal rats or by tracings with multiple lipophilic carbocyanine dyes placed along the dorsoventral axis of the snout. Briefly, trigeminal fibers carrying information from dorsal whisker rows are situated ventrally in the tract, and those carrying information from ventral whisker rows are located dorsally in the tract (Bates and Killackey 1985; Erzurumlu and Jhaveri 1992). There is also evidence suggesting that the rostrocaudal axis of the whisker pad is represented along the mediolateral axis of the TrV and PrV (Bates and Killackey 1985; Belford and Killackey 1980; Erzurumlu and Killackey 1983).

For all barrelette cells, stimulation of the TrV evoked an EPSP followed by a long-lasting IPSP (Fig. 5*B*, $n = 26$). Occasionally, the IPSP was followed by a rebound Na^+ spike (Fig. 5*C*). We saw no evidence of rebound low-threshold spiking confirming that barrelette cells lack I_T. The IPSP reversed in polarity during membrane hyperpolarization (*top traces* vs. *bottom traces* in Fig. 5, *B* and *C*). Interestingly, the evoked responses depended on the location of the stimulation site. We marked the stimulating site near the recorded cell as *site 2* and the site far from the recorded cell as *site 1* (Fig. 5*A*). Stimulation of *site 1* evoked a single IPSP (Fig. 5*D*), and stimulation of *site 2*, at the same intensity, elicited an EPSP-IPSP sequence (Fig. 5*E*).

We also analyzed the pharmacology of these postsynaptic potentials. In barrelette cells, stimulation of *site 1* evoked an IPSP alone (Fig. 5*G*, *trace 1*) that was completely blocked by application of bicuculline (10 μM, Fig. 5*G*, *trace 2*). Thus the IPSP is exclusively mediated by $GABA_A$ receptors. Stimulation of *site 2* induced an EPSP-IPSP sequence (Fig. 5*H*). Blocking $GABA_A$ receptors by bicuculline (10 μM) revealed a long-lasting EPSP (Fig. 5*H*, *trace 1* vs. *2*, $n = 15$). The late component of the EPSP was blocked by D-APV (50 μM, Fig.

5*I*, *trace 1* vs. *2*, $n = 4$). Therefore the EPSP is mediated by both NMDA and nonNMDA type of glutamate receptors. The evoked responses also depended on the stimulus intensity. As shown in Fig. 5, *J–L*, stimulation of *site 1* with lower intensity induced a pure IPSP (Fig. 5*J*), whereas stronger stimulus evoked an EPSP-IPSP sequence (Fig. 5, *J* and *K*), the latter was probably caused by current spread in the TrV. These results indicate that the excitatory and inhibitory responses originate from different trigeminal inputs. This interpretation is supported by the following result. A progressive increase of stimulus intensity produced a stepwise increase in IPSP amplitude (Fig. 5, *F* and *L*). The number of steps suggests that a single barrelette cell receives inhibitory inputs that result from activation of at least five to seven trigeminal nerve fibers. In contrast, increasing stimulus intensity produced either little or no change (Fig. 5*F*) or an increase at two to three steps in EPSP amplitude (Fig. 5*L*, *inset*). This implies that barrelette cells receive inhibition originating from more trigeminal tract fibers than those for excitation.

In response to different stimulus intensities, the latency of the EPSP was nearly constant, suggesting that barrelette cells receive monosynaptic excitation from the trigeminal nerve. The latency of the IPSP was 0.7–0.9 ms longer than that of the EPSP. Because the experiments were conducted at room temperature, 0.7–0.9 ms may account for an extra synaptic delay. The IPSP is most likely mediated by a disynaptic circuit, namely a feed-forward inhibitory circuit.

Synaptic responses of interbarrelette cells

Interbarrelette cells ($n = 12$) responded to TrV stimulation with a long-lasting EPSP. A small IPSP was superimposed on the peak of the EPSP (*top trace* of Fig. 6*A*). The IPSP was reversed at hyperpolarized potential (*bottom trace* of Fig. 6*A*) and blocked by bicuculline (10 μM, Fig. 6*B*, $n = 6$). Additional application of D-APV (50 μM) blocked the late components of the EPSPs, which were induced by either weak (*top traces*) or strong stimulation (*bottom traces* in Fig. 6*C*, $n = 3$). A progressive increase of stimulus intensity caused a stepwise increase in EPSP amplitude. This could be observed in the presence (Fig. 6*D*) or absence (Fig. 7) of bicuculline. Stimulation of TrV at different sites or lower intensity induced an IPSP alone in interbarrelette cells (Fig. 7*A*, $n = 3$). Along with a progressive increase in stimulus intensity, the IPSP gave way to a long-lasting EPSP (Fig. 7, *B–F*). As shown in Fig. 7*G*, an increase in stimulus intensity produced a stepwise increase in EPSP amplitude and eventually masked the IPSP. From the number of steps, we can estimate that a single interbarrelette cell receives excitatory inputs from at least five to seven trigeminal nerve fibers ($n = 6$). In response to different stimulus intensities, the latency of the EPSP remained constant (Figs. 6*D* and 7*G*). This suggests that interbarrelette cells receive monosynaptic excitation from whisker afferents. The latency of the IPSP was about one synaptic delay (0.7–0.9 ms) longer than the EPSP. Thus the IPSP is mediated by a disynaptic circuit. In three interbarrelette cells, an increase in stimulus intensity evoked another polysynaptic EPSP (Fig. 7, *C* and *H*). When strong stimulus intensities were used, the late polysynaptic EPSP merged with the monosynaptic EPSP (Fig. 7*G*).

DISCUSSION

Previous studies documented morphological features of projection cells and interneurons of the adult rat brain stem trigeminal complex and correlated them with peripherally driven response characteristics (Arends and Jacquin 1993; Jacquin et al. 1986, 1988, 1989a,b; Jacquin and Renehan 1995). However, little is known about the nature of synaptic transmission during a time when brain stem trigeminal neurons are consolidating whisker-specific patterns. In recent years, neural activity, via NMDA receptors have been noted as a major player in whisker-specific pattern formation in the trigeminal brain stem. Gene deletion or transgenic alterations of receptor subunit function studies have underscored the

role of NMDA receptors in this process (Iwasato et al. 1997; Kutsuwada et al. 1996; Li et al. 1994). NMDA receptors are abundant in the trigeminal brain stem complex during pattern formation (Iwasato et al. 1997; Rema and Ebner 1996). The present study shows that both barrelette and interbarrelette cells receive trigeminal input mediated by NMDA and non-NMDA receptors. In addition, for barrelette cells, the NMDA receptor–mediated EPSP is masked by a $GABA_A$ receptor–mediated IPSP. Inhibitory synaptic responses and intrinsic membrane properties of neurons are thought to play a crucial role in pattern formation (Erzurumlu and Guido 1996). These properties reflect the manner in which pattern forming cells respond to their synaptic inputs and how they relay pattern-related information to neurons leading to the somatosensory cortex.

Electrophysiological recordings in adult rat brain stem trigeminal nuclei show that barrelette cells are unique in their function, such that they have only single whisker receptive fields. Other relay neurons and interbarrelette cells respond to stimulation of multiple whiskers (Jacquin et al. 1986, 1988, 1989a,b; Shipley 1974). Studies combining retrograde labeling techniques and immunohistochemistry document that different classes of BSTC neurons can be distinguished from one another by their expression of parvalbumin, calbindin, and GABA (Bennett-Clarke et al. 1992; Haring et al. 1990). On the other hand, hardly anything is known about these cells during the sensitive period for pattern formation. In this study we found that in the PrV of 4- to 12-day-old rat pups three different cell types can be readily identified: barrelette, interbarrelette, and GABAergic cells (see also Arends and Jacquin 1993; Ginestal and Matute 1993; Ma 1991, 1993). We further show that morphologically identified barrelette cells have a prominent I_A and interbarrelette cells have a prominent I_T. Thus we can identify cell types in the PrV by their active conductances during the first postnatal week. Ongoing studies are aimed at defining electrophysiological properties of PrV neurons during earlier developmental periods.

Based on our current observations, we propose the following neuronal circuitry for the early postnatal PrV (Fig. 8). Barrelette cells exhibit a monosynaptic EPSP followed by a disynaptic IPSP after stimulation of the TrV. Because the stimulation threshold of the EPSP and that of the IPSP are about the same, they may originate from the same trigeminal input. The disynaptic IPSP must be mediated by a feed-forward inhibitory circuit as shown in Fig. 8 (whisker 1 pathway). GABAergic cells in the PrV most likely serve as inhibitory interneurons in this feed-forward circuit. An IPSP without the preceding EPSP can be evoked in barrelette cells by stimulating different sites in the TrV, suggesting that there is a separate inhibitory circuit other than the feed-forward inhibitory circuit. In addition, barrelette cells seem to receive more inhibitory inputs than excitatory ones. Collectively, these results suggest that some trigeminal fibers only activate the inhibitory circuits that feed to a given barrelette cell. Because the IPSP has a disynaptic latency, it is most likely mediated via lateral inhibitory circuitry. Namely, activation of one pathway produces inhibition in other parallel pathways. The organization of dendritic trees, and receptive fields of the barrelette cells indicate that each cell receives excitatory afferent inputs mainly from a single whisker. Because the TrV fibers are topographically organized (Bates and Killackey 1985; Erzurumlu and Jhaveri 1992; Erzurumlu and Killackey 1983), we can deduce that barrelette cells receive disynaptic lateral inhibition from neighboring whiskers (Fig. 8, whisker 2 pathway). Both feed-forward and lateral inhibition must play a crucial role in determining spatial and temporal response properties of barrelette cells. The lateral inhibition from neighboring whiskers sharpens the receptive field of a given barrelette cell. Most likely, this provides barrelette cells with a center-surround receptive field organization, similar to that seen in the retina (Cook and McReynolds 1998). The IPSP with a delay of 0.7–0.9 ms curtails the preceding EPSP, so that the excitatory response in barrelette cells becomes phasic (short-lasting). The duration of the IPSP may be modulated by both I_A (to prolong) and I_H (to shorten), so that the IPSP is kept at a constant duration (~150 ms in our

case). Such control may be critical for the temporal resolution of responses along the trigeminothalamic pathway (Hartings and Simons 1998).

A stepwise increase in EPSP (or IPSP) amplitude evoked by increased stimulus intensity has been observed in other brain structures. It most probably indicates successive recruitment of additional fibers and therefore an increase in the number of active synapses (Allen et al. 1977; Bartlett and Smith 1999; Mock et al. 1997). Although this approach cannot provide the exact number of afferent fibers, it serves as a useful means to estimate afferent convergence. For barrelette cells, there appears to be a greater convergence in the inhibitory circuit than in the excitatory circuit. In contrast, for interbarrelette cells there seems to be greater convergence in the excitatory circuit than in the inhibitory circuit. Most probably, interbarrelette cells receive monosynaptic excitation from multiple whiskers (Fig. 8, whisker 1 and 3 pathways). This is in accord with other studies showing that the receptive field of interbarrelette cells are much larger than those of barrelette cells (Jacquin et al. 1986, 1988, 1989a,b; Shipley 1974). These cells may also receive inputs from other barrelette and/or interbarrelette cells. Although interbarrelette cells receive a weak lateral inhibition, the convergence of excitatory inputs reflects the level of activation of the PrV. Because interbarrelette cells project to other subnuclei within the BSTC (Jacquin et al. 1990; Nasution and Shigenaga 1987), their main function may be to coordinate the activity of different brain stem trigeminal subnuclei, and to modulate transmission of afferent inputs to a variety of projection sites. In a recent study Sandler et al. (1998) reported bursting cells with an elongated dendritic field and Ni^{2+}-blocked (most likely T-type) Ca^{2+} conductance in the PrV of the gerbil. Although this study did not note the location of the cells recorded from in the PrV, these cells appear similar to morphologically identified interbarrelette cells described in the present study.

Within the rodent BSTC, PrV barrelette cells are the key players in conveying whisker-related patterns to the dorsal thalamus (Killackey and Fleming 1985). However, in two subnuclei of the spinal trigeminal nucleus (subnuclei interpolaris and caudalis), whisker-related patterns, i.e., barrelettes, are also present. In fact, the most conspicuous barrelettes of the BSTC are found in the subnucleus interpolaris (SPI). Recent work from our laboratory showed that I_H, I_T, and I_A are present in SPI neurons as well (Guido et al. 1998). However, we have not yet correlated these conductances with morphologically identified specific cell types. Therefore we do not know whether barrelette and interbarrelette cells of the SPI also exhibit class-specific conductances like the cells of the PrV.

Collectively, our results from studies on the PrV and SPI suggest that unique combinations of electrophysiological properties of the developing BSTC neurons could enhance activity-dependent modeling of neural connections during pattern formation. Electrophysiological properties of barrelette cells are especially suited for detection of patterned trigeminal inputs from the whiskers and the transmittal of pattern-related information to the barreloids of the dorsal thalamus with sharpened receptive field and phasic temporal properties. Interbarrelette cells with “diffuse”projections to other upstream trigeminal-recipient brain regions sample excitatory inputs from multiple whiskers and barrelette cells.

Acknowledgments

We thank T. Ulupinar for help with histology and manuscript preparation and Dr. E. Ulupinar for help with immunohistochemistry.

This project was supported by the Whitehall Foundation and by National Institute of Neurological Disorders and Stroke Grant NS-37070 to R. S. Erzurumlu.

REFERENCES

Allen GI, Oshima T, Toyama K. The mode of synaptic linkage in the cerebro-ponto-cerebellar pathway investigated with intracellular recording from pontine nuclei cells of the cat. Exp. Brain Res. 1977; 29:123–136. [PubMed: 196876]

Arends JA, Jacquin MF. Lucifer Yellow staining in fixed brain slices: optimal methods and compatibility with somatotopic markers in neonatal brain. J. Neurosci. Methods. 1993; 50:321–339. [PubMed: 8152243]

Bartlett EL, Smith PH. Anatomic, intrinsic synaptic properties of dorsal and ventral division neurons in rat medial geniculate body. J. Neurophysiol. 1999; 81:1999–2016. [PubMed: 10322042]

Bates CA, Killackey HP. The organization of the neonatal rat's brainstem trigeminal complex and its role in the formation of central trigeminal patterns. J. Comp. Neurol. 1985; 240:265–287. [PubMed: 2999198]

Belford GR, Killackey HP. Vibrissae representation in subcortical trigeminal centers of the neonatal rat. J. Comp. Neurol. 1979; 183:305–322. [PubMed: 762261]

Belford GR, Killackey HP. The sensitive period in the development of the trigeminal system of the neonate rat. J. Comp. Neurol. 1980; 193:335–350. [PubMed: 7440771]

Bennett-Clarke CA, Chiaia NL, Jacquin MF, Rhoades RW. Parvalbumin and calbindin immunocytochemistry reveal functionally distinct cell groups and vibrissa-related patterns in the trigeminal brainstem complex of the adult rat. J. Comp. Neurol. 1992; 320:323–338. [PubMed: 1377200]

Blanton MG, Turco JJL, Kriegstein AR. Whole cell recording from neurons in slices of reptilian and mammalian cerebral cortex. J. Neurosci. Methods. 1989; 30:203–210. [PubMed: 2607782]

Chiaia NL, Bennett-Clarke CA, Eck M, White FA, Crissman RS, Rhoades RW. Evidence for prenatal competition among the central arbors of trigeminal primary afferent neurons. J. Neurosci. 1992; 12:62–76. [PubMed: 1309577]

Cook PB, McReynolds JS. Lateral inhibition in the inner retina is important for spatial tuning of ganglion cells. Nature Neurosci. 1998; 1:714–719. [PubMed: 10196588]

Durham D, Woolsey TA. Effects on neonatal whisker lesions on mouse central trigeminal pathways. J. Comp. Neurol. 1984; 233:424–447. [PubMed: 6707253]

Erzurumlu RS, Bates CA, Killackey HP. Differential organization of the thalamic projection cells in the brainstem trigeminal complex of the rat. Brain Res. 1980; 193:427–433. [PubMed: 7388601]

Erzurumlu, RS.; Guido, W. Cellular mechanisms underlying the formation of orderly connections in developing sensory pathways. In: Mize, RR.; Erzurumlu, RS., editors. Progress in Brain Research. Neural Development and Plasticity. Vol. vol. 108. Elsevier; Amsterdam: 1996. p. 287-301.

Erzurumlu RS, Jhaveri S. Thalamic axons confer a blueprint of the sensory periphery onto the developing rat somatosensory cortex. Dev. Brain Res. 1990; 56:229–234. [PubMed: 2261684]

Erzurumlu RS, Jhaveri S. Trigeminal ganglion cell processes are spatially ordered prior to the differentiation of the vibrissa pad. J. Neurosci. 1992; 12:3946–3955. [PubMed: 1403092]

Erzurumlu RS, Killackey HP. Diencephalic projections of the subnucleus interpolaris of the brainstem trigeminal complex in the rat. Neuroscience. 1980; 5:1891–1901. [PubMed: 7432628]

Erzurumlu, RS.; Killackey, HP. Defining critical and sensitive periods in neurobiology. In: Hunt, RK., editor. Current Topics in Developmental Biology. Neural Development. Part III. Vol. vol. 17. Academic; New York: 1982. p. 207-240.

Erzurumlu RS, Killackey HP. Development of order in the rat trigeminal system. J. Comp. Neurol. 1983; 213:365–380. [PubMed: 6601119]

Erzurumlu RS, Lo F-S. Electrophysiological properties and synaptic responses of rat principal nucleus cells during development and following denervation. Soc. Neurosci. Abstr. 1999; 25:222.

Ferster D, Jagadeesh B. EPSP-IPSP interactions in cat visual cortex studied with in vivo whole-cell patch recording. J. Neurosci. 1992; 12:1262–1274. [PubMed: 1556595]

Ginestal E, Matute C. Gamma-aminobutyric acid–immunoreactive neurons in the rat trigeminal nuclei. Histochemistry. 1993; 99:49–55. [PubMed: 8468194]

Guido W, Gunhan-Agar E, Erzurumlu RS. Developmental changes in the electrophysiological properties of brain stem trigeminal neurons during pattern (barrelette) formation. J. Neurophysiol. 1998; 79:1295–1306. [PubMed: 9497411]

Haring JH, Henderson TA, Jacquin MF. Principalis- or parabrachial-projecting spinal trigeminal neurons do not stain for GABA or GAD. Somatosens. Mot. Res. 1990; 7:391–397. [PubMed: 1963251]

Hartings JA, Simons DJ. Thalamic relay of afferent responses to 1- to 12-Hz whisker stimulation in the rat. J. Neurophysiol. 1998; 80:1016–1019. [PubMed: 9705491]

Ivy GO, Killackey HP. The ontogeny of the distribution of callosal projection neurons in the rat parietal cortex. J. Comp. Neurol. 1981; 195:367–389. [PubMed: 6162864]

Iwasato T, Erzurumlu RS, Huerto PT, Chen DF, Sasaoka T, Ulupinar E, Tonegawa S. NMDA Receptor-dependent refinement of somatotopic maps. Neuron. 1997; 19:1–20. [PubMed: 9247258]

Jacquin MF, Barcia M, Golden J, Rhoades RW. Structure-function relationships in rat brainstem subnucleus interpolaris. IV. Projection neurons. J. Comp. Neurol. 1989a; 282:45–62. [PubMed: 2708593]

Jacquin MF, Chiaia NL, Haring JH, Rhoades RW. Intersubnuclear connections within the rat trigeminal brainstem complex. Somatosens. Mot. Res. 1990; 7:399–420. [PubMed: 2291376]

Jacquin MF, Golden J, Panneton WM. Structure and function of barrel “precursor” cells in trigeminal nucleus principalis. Dev. Brain Res. 1988; 43:309–314.

Jacquin MF, Golden J, Rhoades RW. Structure-function relationships in rat brainstem subnucleus interpolaris. III. Local circuit neurons. J. Comp. Neurol. 1989b; 282:24–44. [PubMed: 2708592]

Jacquin MF, Mooney RD, Rhoades RW. Morphology, response properties, and collateral projections of trigeminothalamic neurons in the brainstem subnucleus interpolaris of rat. Exp. Brain Res. 1986; 61:457–468. [PubMed: 3007189]

Jacquin MF, Renehan WE. Structure-function relationships in rat brainstem subnucleus interpolaris. XII. Neonatal deafferentation effects on cell morphology. Somatosens. Mot. Res. 1995; 12:209–233. [PubMed: 8834299]

Jhaveri, S.; Erzurumlu, RS. Two phases of pattern formation in the developing rat trigeminal system. In: Sharma, SC.; Goffinet, AM., editors. Development of the Central Nervous System in Vertebrates. Plenum; New York: 1992. p. 167-178.

Killackey HP, Fleming K. The role of the principal sensory nucleus in central trigeminal pattern formation. Dev. Brain Res. 1985; 22:141–145.

Kutsuwada T, Sakimura K, Manabe T, Takayama C, Katakura N, Kushiya E, Natsume R, Watanabe M, Inoue Y, Yagi T, Aizawa S, Arakawa M, Takahashi T, Nakamura Y, Mori H, Mishina M. Impairment of suckling response, trigeminal neuronal pattern formation, and hippocampal LTD in NMDA receptor e2 subunit mutant mice. Neuron. 1996; 16:333–344. [PubMed: 8789948]

Li Y, Erzurumlu RS, Chen C, Jhaveri S, Tonegawa S. Whisker-related neuronal patterns fail to develop in the brainstem trigeminal nuclei of NMDAR1 knockout mice. Cell. 1994; 76:427–437. [PubMed: 8313466]

Ma PM. The barrelettes—architectonic vibrissal representations in the brainstem trigeminal complex of the mouse. I. Normal structural organization. J. Comp. Neurol. 1991; 309:161–199. [PubMed: 1715890]

Ma PM. Barrellettes: architectonic vibrissal representations in the brainstem trigeminal complex of the mouse. II. Normal postnatal development. J. Comp. Neurol. 1993; 327:376–397. [PubMed: 8440772]

Ma PM, Woolsey TA. Cytoarchitectonic correlates of the vibrissae in the medullary trigeminal complex of the mouse. Brain Res. 1984; 306:374–379. [PubMed: 6205721]

Mock M, Schwarz C, Thier P. Electrophysiological properties of rat pontine nuclei neurons in vitro. II. Postsynaptic potentials. J. Neurophysiol. 1997; 78:3338–3350. [PubMed: 9405548]

Nasution ID, Shigenaga Y. Ascending and descending internuclear projections within the trigeminal sensory nuclear complex. Brain. Res. 1987; 425:234–247. 10. [PubMed: 2827843]

Neher E. Correction for liquid junction potentials in patch clamp experiments. Methods Enzymol. 1992; 207:123–131. [PubMed: 1528115]

O'Leary DDM, Ruff NL, Dyck RH. Development, critical period plasticity, and adult reorganizations of mammalian somatosensory systems. Curr. Opin. Neurobiol. 1994; 4:535–544. [PubMed: 7812142]

Rema V, Ebner FF. Postnatal changes in NMDAR1 subunit expression in the rat trigeminal pathway to barrel field cortex. J. Comp. Neurol. 1996; 368:165–184. [PubMed: 8725300]

Sandler VM, Puil E, Schwarz DW. Intrinsic response properties of bursting neurons in the nucleus principalis trigemini of the gerbil. Neuroscience. 1998; 83:891–904. [PubMed: 9483572]

Senft SL, Woolsey TA. Growth of thalamic afferents into mouse barrel cortex. Cereb. Cortex. 1991; 1:308–335. [PubMed: 1822738]

Shipley MT. Response characteristics of single units in the rat's trigeminal nuclei to vibrissa displacements. J. Neurophysiol. 1974; 37:73–90. [PubMed: 4359792]

Van Der Loos H. Barreloids in mouse somatosensory thalamus. Neurosci. Lett. 1976; 2:1–6. [PubMed: 19604804]

Wong-Riley MT, Welt C. Histochemical changes in cytochrome oxidase of cortical barrels after vibrissal removal in neonatal and adult mice. Proc. Natl. Acad. Sci. USA. 1980; 77:2333–2337. [PubMed: 6246540]

Woolsey, TA. Peripheral alteration and somatosensory development. In: Coleman, EJ., editor. Development of Sensory Systems in Mammals. Wiley; New York: 1990. p. 461-516.

Woolsey TA, Van Der Loos H. The structural organization of layer IV in the somatosensory region (SI) of mouse cerebral cortex. Brain Res. 1970; 17:204–242.

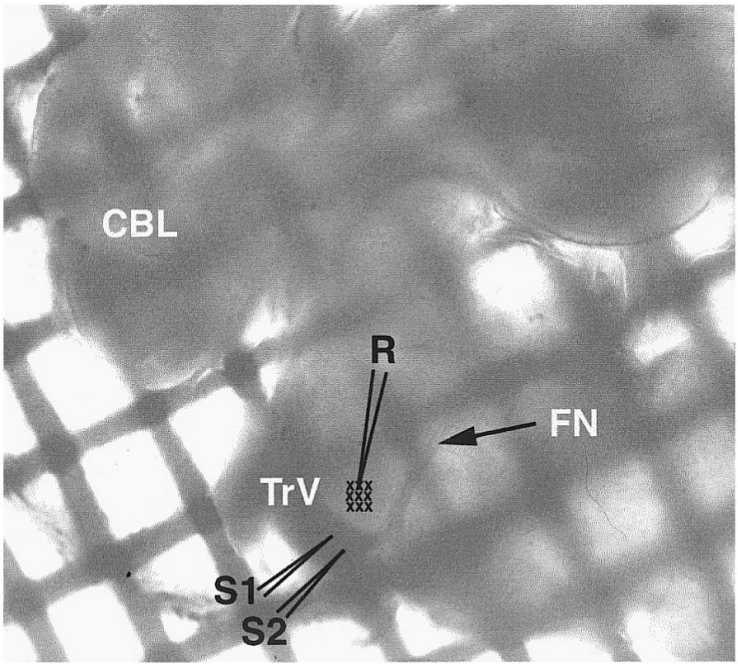

FIG. 1.

Low-power photomicrograph of a freshly dissected brain stem slice from a *postnatal day 6* (*PND 6*) rat pup within the recording chamber. The trigeminal tract (TrV) and the principal sensory nucleus (PrV) are readily visible and the stimulating (S1 and S2) and recording (R) sites are sketched on the photomicrograph. Barrelette region is also indicated (small crosses). FN, root of the facial nerve; CBL, cerebellum. The slice lies over a nylon mesh grid, mesh size = 500 μm^2.

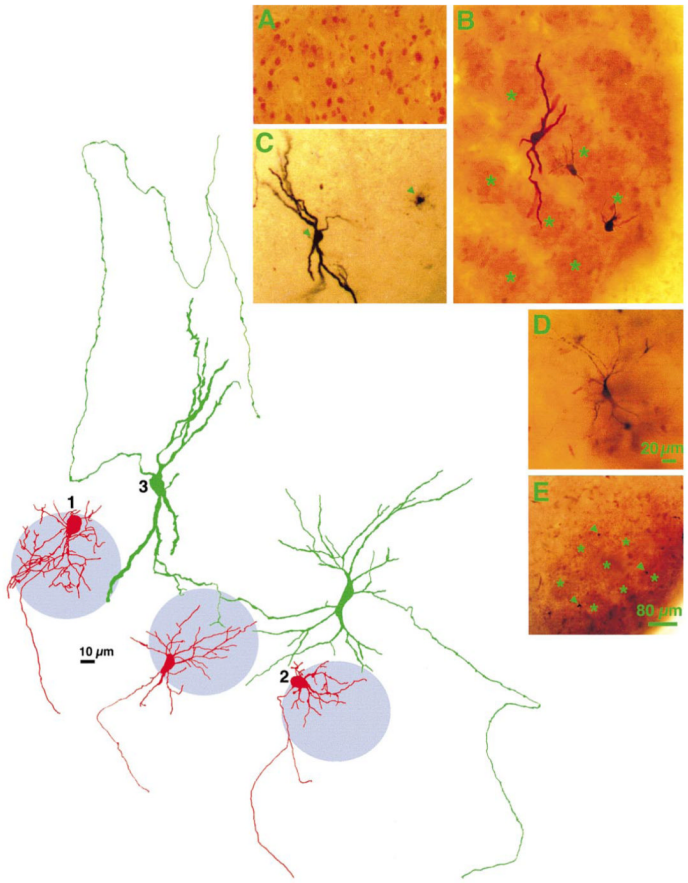

FIG. 2.

Examples of physiologically and morphologically identified barrelette and interbarrelette neurons from the PrV of *PND5–8* rats. *A*: GABA immunopositive PrV cells in the barrelette region. Note their small size in comparison to barrelette and interbarrelette cells. *B*: cytochrome oxidase histochemistry and biocytin-filled cells superimposed. Note the large interbarrelette cell with extensive dendritic tree and the barrelette cells with small dendritic trees confined to single barrelettes. Asterisks mark the center of individual barrelettes. *C*: biocytin-labeled interbarrelette cell. *D*: biocytin-labeled barrelette cell. *E*: location of biocytin-labeled barrelette cells (arrowheads) in a cytochrome oxidase stained PrV slice (asterisks mark individual barrelettes). The camera lucida drawings of barrelette cells (red) and interbarrelette cells (green) show the orientation of their dendritic fields with respect to barrelette patches (violet circles).

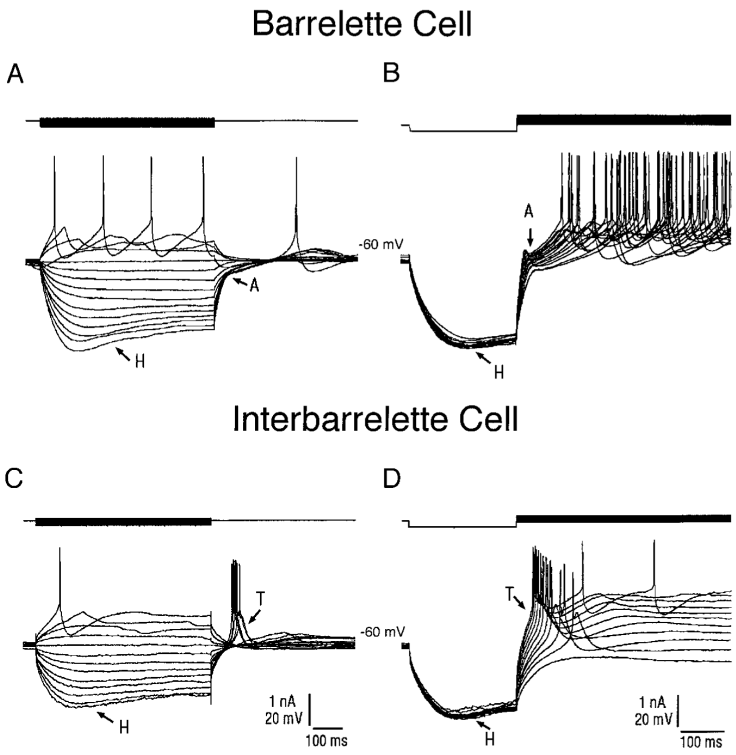

FIG. 3.

Physiological classification of barrelette and interbarrelette neurons. *A* and *B*: voltage responses of a barrelette neuron (shown in Fig. 2, *cell 1*) to intracellular current injection. *Top traces*: current pulses. *Bottom traces*: voltage responses. *A*: strong hyperpolarization activates a mixed cation conductance (H), which produces a depolarizing "sag" in the response. Note the long hyperpolarizing tail (A) on cessation of the hyperpolarizing current pulse. This response reflects the activation of an A-type conductance. *B*: activation of A-type conductance is also evident at different depolarizing levels following membrane hyperpolarization. Note the hyperpolarizing notch (A) that delays the generation of action potentials. *C* and *D*: voltage responses of an interbarrelette neuron (shown in Fig. 2*B*, *cell 3*) to intracellular current injection. *C*: interbarrelette cell also shows a depolarizing "sag" (H) during strong hyperpolarization. On termination of the hyperpolarizing pulses, the passive repolarization of the membrane triggers a rebound low-threshold Ca^{2+} spike (T) that contains a burst of action potentials riding its peak. *D*: low-threshold Ca^{2+} spikes are also triggered by membrane depolarization from hyperpolarized levels. Barrelette neurons possess prominent H and A-type conductances, whereas interbarrelette neurons, in addition to H, also possess a prominent low-threshold Ca^{2+} conductance.

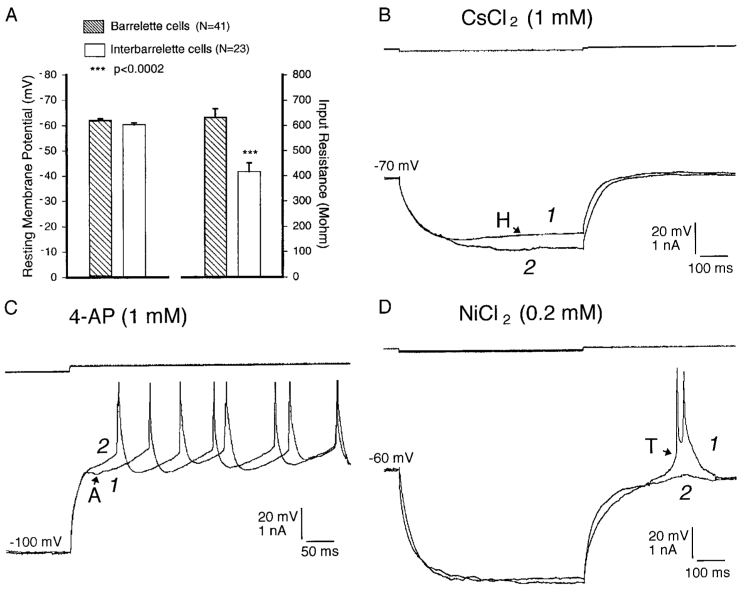

FIG. 4.

Membrane properties of barrelette and interbarrelette neurons. *A*: passive membrane properties of 41 barrelette and 23 interbarrelette neurons. Bar: mean value; error bar: standard error. There is no significant difference in resting membrane potentials between the 2 classes ($P > 0.08$). However, the input resistance of barrelette cells is significantly higher than that of interbarrelette cells ($P < 0.0002$). *B*: I_H is blocked by $CsCl_2$ (1 mM). *Trace 1*, before; *trace 2*, after drug application. The same sequence for the ensuing figures. *C*: I_A is blocked by 4-aminopyridine (4-AP; 1 mM). *D*: I_T is largely blocked by $NiCl_2$ (0.2 mM).

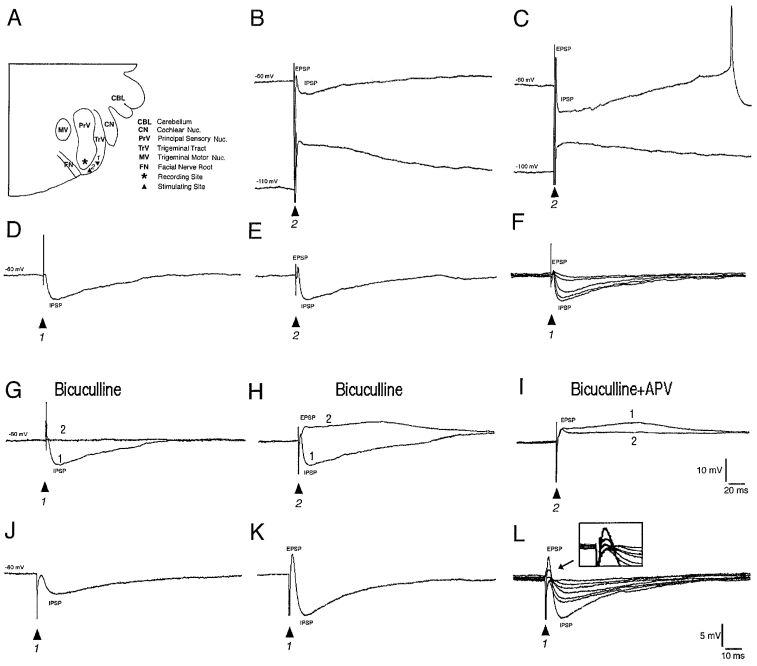

FIG. 5.

Synaptic responses of barrelette neurons to stimulation of the trigeminal tract (TrV). *A*: diagrammatic illustration of the brain stem slice indicating the stimulation and recording sites. The stimulation site near the recorded cell is marked as *site 2*, whereas the site far from the recorded cell as *site 1. B* and *C*: postsynaptic potentials at different membrane potentials. In every barrelette cell tested, stimulation of TrV (arrowheads) evokes a short excitatory postsynaptic potential (EPSP) and a long-lasting inhibitory postsynaptic potential (IPSP). Note that the IPSP has reversed in polarity at hyperpolarized levels (*bottom traces* in *B* and *C*). Sometimes the IPSP is followed by a rebound single spike (*C*). *D*: stimulation of *site 1* evokes an IPSP alone. *E*: stimulation of *site 2* at the same intensity evokes an EPSP-IPSP sequence. *G*: in another barrelette cell, stimulation of *site 1* evokes an IPSP. The IPSP is completely blocked by application of bicuculline (10 μM, *1* vs. *2*). *H*: stimulation of *site 2* at the same intensity induces an EPSP-IPSP sequence. Bicuculline blocks the IPSP and significantly prolongs the EPSP (*1* vs. *2*). *I*: subsequent application of D-2-amino-5-phosphonovaleric acid (D-APV; 50 μM) blocks the late component of the EPSP (*1* vs. *2*). *J–L*: in another barrelette cell, weak stimulus (0.3 ms, 0.3 mA) evokes a pure IPSP. An increase in stimulus intensity (0.3 ms,0.6 mA) at the same site evokes an EPSP-IPSP sequence. *F*: a progressive increase of stimulus intensity (from 0.05 to 1.0 mA, 0.3 ms) produces little change in EPSP amplitude but a stepwise increase in IPSP amplitude. *L*: a progressive increase of stimulus intensity (from 0.05 to 0.6 mA, 0.3 ms) produces a 3-step increase in EPSP amplitude (see *inset*), whereas a 7-step increase in IPSP amplitude. These results suggest that barrelette cells receive excitatory input from one whisker and extensive lateral inhibition from neighboring whiskers. Note that *D–F, G–I*, and *J–L* show recordings from 3 different cells.

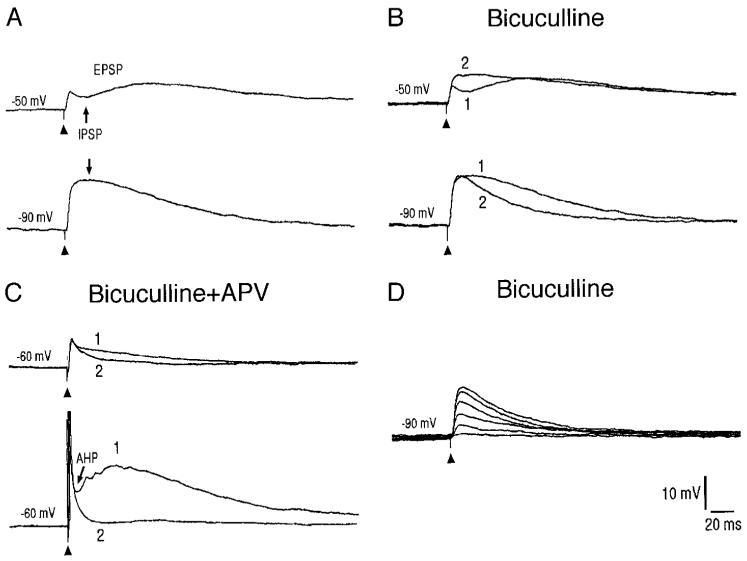

FIG. 6.

Synaptic responses of interbarrelette cells to stimulation of TrV. *A*: stimulation of TrV evokes a long-lasting EPSP and a small IPSP that has reversed at −90 mV. The membrane potential is held at either −50 mV to increase IPSP amplitude or at −90 mV to reverse the IPSP. *B*: IPSPs at different membrane potentials are blocked by application of bicuculline (10 μM, *1* vs. *2*). *C*: the late component of the EPSP induced by either weak (*top trace*) or strong (*bottom trace*) stimulation, is blocked by additional application of D-APV (50 μM, *1* vs. *2*). *D*: a progressive increase in stimulus intensity (from 0.05 to 0.9 mA) produces a stepwise increase in EPSP amplitude suggesting that interbarrelette cells receive excitatory inputs from several whiskers.

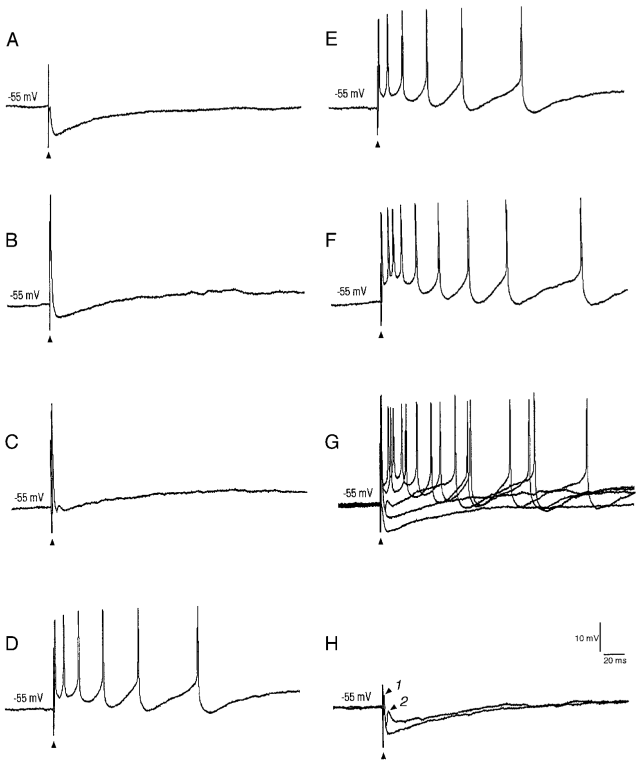

FIG. 7.

Synaptic inputs of interbarrelette cells. *A–F*: synaptic responses of an interbarrelette cell to a progressive increase in stimulus intensity. *A*: at or near threshold, stimulation evokes a pure IPSP. *B* and *C*: stimulation at moderate intensities induces an earlier EPSP with single sodium spike and a late IPSP. *D–F*: stronger stimulation elicits a long-lasting EPSP with a train of spikes. *G*: superimposed traces from *B–F* underscore how the IPSP gives way to the long-lasting EPSP along with progressive increases in stimulus intensity. *H*: a slight increase in stimulus intensity may also evoke a late EPSP (*2*) that follows the initial EPSP (*1*). This late EPSP can be also evident in the records of *C* and *G* (*middle trace*).

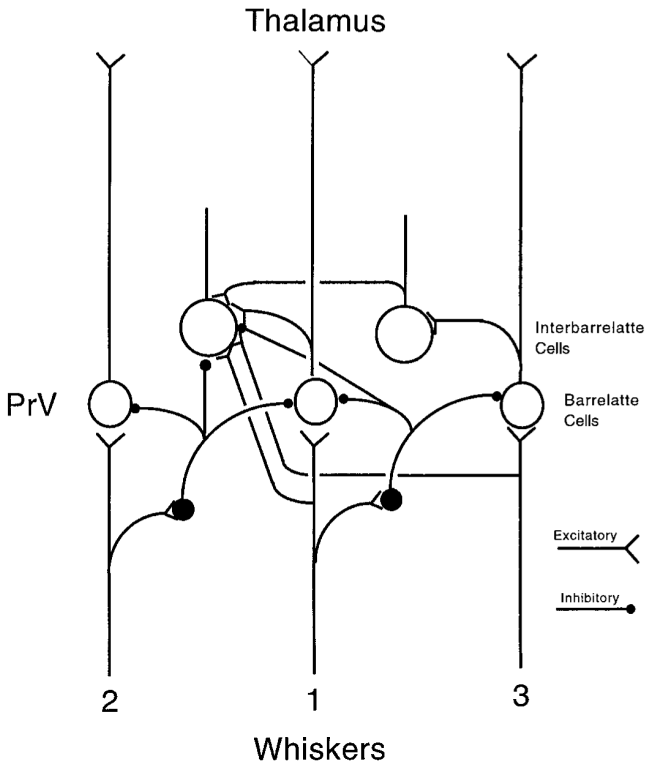

FIG. 8.

Neuronal circuitry in the trigeminal principal sensory nucleus. Proposed wiring diagram depicting synaptic organization in the PrV. Barrelette cells receive monosynaptic excitation largely from one whisker, disynaptic feed-forward inhibition from the same whisker, and lateral inhibition probably from neighboring whiskers. Interbarrelette cells receive monosynaptic excitation from several whiskers and polysynaptic excitation presumably from other interbarrelette cells or barrelette cells. Interbarrelette cells also receive a weak lateral inhibition.